Mass Preserving Finite Element Implementations of Level Set Method

Daniele A. Di Pietro [a], Stefania Lo Forte [b] and Nicola Parolini [c]

[a] *Dipartimento di Ingegneria Industriale, Università di Bergamo, Italy, dipietro@unibg.it*

[b] *MOX, Politecnico di Milano, Italy, stefania.loforte@mate.polimi.it*

[c] *Institut d'Analyse et Calcul Scientifique, EPFL Lausanne, Switzerland, nicola.parolini@epfl.ch*

Abstract

In the last two decades, the level set method has been extensively used for the numerical solution of interface problems in different domains. The basic idea is to embed the interface as the level set of a regular function. In this paper we focus on the numerical solution of hyperbolic interface advection equations which appears in free-surface fluid dynamics problems, where *naïve* finite element implementations are unsatisfactory. As a matter of fact, practitioners in fluid dynamics often complain that the mass of each fluid component is not conserved, a phenomenon which is therefore often referred to as *mass loss*. In this paper we propose and compare two finite element implementations that cure this ill-behaviour without the need to resort to spurious strategies (such as, *e.g.*, particle level set). The first relies on a discontinuous Galerkin discretization, which is known to give very good performance when facing hyperbolic problems; the second is a stabilized continuous FEM implementation based on the stabilization method presented in [1], which is free from many of the problems that classical methods exhibit when applied to unsteady problems.

1 Introduction

The problem of interface evolution is one of tracking the motion of an interface as it evolves. Many techniques have been developed to this purpose. Among these we recall: particle tracking, which consists in following a finite number of particles and reconstructing the front as an interpolation of particle positions at each time step; volume-of-fluid technique, which stems from the field of multi-fluid CFD, and accounts for the fraction of the two fluids in each volume rather than explicitly tracking the interface; level set technique, which

embeds the front at time t as the zero level set of a regular function defined all over the integration domain. Under some assumptions on the dependence of the velocity, the level set method requires the solution of a Hamilton-Jacobi equation.

All these methods suffer from particular problems. A major difficulty in particle tracking techniques is the handling of topological changes of the front (coalescence and splitting). A critical point in volume of fluid technique is front reconstruction, since the only available information is the fraction of both fluids inside each volume. Inaccuracy in front reconstruction may lead to even greater inaccuracy in the computation of physically significant quantities like the normal and the curvature of the interface. While solving these problems in a very elegant way, the level set method too has some drawbacks. As a matter of fact, many of the techniques employed in the solution of Hamilton-Jacobi or hyperbolic problems prove inadequate when applied to the level set equation. In particular, when considering finite element discretizations, it is widely known that a certain amount of numerical viscosity has to be added in order to stabilize the numerical solution. While acceptable in other cases, this artificial diffusion might be too big to achieve sufficient accuracy in following the evolution of a certain level set of a function. The related phenomenon is often referred to as *mass loss* because its most remarkable consequence is that the amount of one fluid diminishes, violating mass conservation. Many modifications of the original scheme have been proposed, often combining finite element discretizations with other techniques: we just recall the particle level set method introduced in [2].

In this work we investigate a cure for the problems outlined above which preserves the original simplicity and mathematical elegance of the level set idea. As regards the first method, the good properties of discontinuous finite element (DG-FE henceforth) approximation of hyperbolic problems are exploited. Many examples in the literature have shown that the amount of artificial viscosity introduced in upwind treatment of interface terms is much smaller than the one needed by stabilization techniques normally applied to continuous element discretizations (see, *e.g.*, [3] and the references therein). In addition, discontinuous Galerkin discretization allows for straightforward implementation of p-adaptivity and non-conforming h-adaptivity. The second method borrows some ideas from the framework of DG-FE methods, achieving stabilization by weakly enforcing a higher regularity on the numerical solution. This is done by penalizing the gradient jumps on inter-element boundaries. Finally, we will report a set of numerical tests that have been carried out to assess the accuracy and robustness of the numerical schemes introduced.

2 The level set method

The idea underlying the level set approach was first proposes by Dervieux and Thomasset in [4], where the interface between two fluids was defined as the zero level set of a *pseudo-density* function. The level set method was introduced by Osher and Sethian in [5] for the numerical solution of front propagating problems with curvature-dependent motion and later extended to a variety of physical applications (a complete introduction can be found in [6]). Consider a boundary moving in a direction normal to itself with a speed F. The key idea is to embed the front at time t as the zero level set of a function $\phi(\mathbf{x}, t)$ defined all over the domain Ω. An evolutive equation is then written for ϕ by imposing that:

- The level set of a point $\mathbf{x}$ belonging to the front at time $t \geq t_0$ be 0, i.e.

$$\phi(\mathbf{x}(t), t) = 0 \quad \forall \mathbf{x} \in \Gamma(t),$$

  being $\Gamma(t) = \{\mathbf{x} \in \Omega : \phi(\mathbf{x}, t) = 0\}$ the front.
- The level set of each point belonging to the front at time t still be 0 at time $t + dt$:

$$\frac{\mathrm{d}\phi}{\mathrm{d}t} = 0 \Rightarrow \frac{\partial \phi}{\partial t} + \dot{\mathbf{x}} \cdot \nabla \phi = 0.$$

Deformation of the front is therefore only due to the normal component of velocity. Hence, by definition we have that $\dot{\mathbf{x}} \cdot \mathbf{n} = F$. Being the front a level set of function ϕ, the normal can be evaluated at each point from:

$$\mathbf{n} = \frac{\nabla \phi(\mathbf{x})}{|\nabla \phi(\mathbf{x})|}, \quad \mathbf{x} \in \Gamma(t).$$

The level set problem therefore becomes:

$$\begin{cases} \frac{\partial \phi}{\partial t} + F |\nabla \phi| = 0 \ \mathbf{x} \in \Omega, \quad t > 0, \\ \phi(\mathbf{x}, t = 0) = \phi_0 \ \mathbf{x} \in \Omega. \end{cases} \tag{1}$$

To understand the connection between the level set problem (1) and the Hamilton-Jacobi equation, suppose that the velocity F depends only upon the position $\mathbf{x}$ and on the first derivatives of ϕ, i. e. $F = F(\mathbf{x}, D\phi)$. Problem (1) can be recast in the following form:

$$\begin{cases} \phi_t + H(\mathbf{x}, D\phi) = 0 \ \mathbf{x} \in \Omega, \quad t > 0, \\ \phi(\mathbf{x}, t = 0) = \phi_0 \qquad \mathbf{x} \in \Omega, \end{cases} \tag{2}$$

where $H(\mathbf{x}, D\phi)$ is the Hamiltonian defined as:

$$H(\mathbf{x}, D\phi) = F |\nabla \phi|.$$

A special case is obtained when the Hamiltonian is a linear function of $\nabla\phi$:

$$H(\mathbf{x},\, D\phi) = \mathbf{b}(\mathbf{x}, t) \cdot \nabla\phi \tag{3}$$

since (2) becomes a linear hyperbolic problem. The physical interpretation of such a problem is that of an interface advected by an given velocity field $\mathbf{b}(\mathbf{x}, t)$. This case is of particular interest in free-surface CFD, since the solution of Navier-Stokes equations and of the front advection problem are often split to reduce complexity. Had the velocity $\mathbf{b}$ depended upon ϕ (but not on its derivatives), we would get a non-linear hyperbolic problem.

Though several choices are possible for the level set function ϕ, the only requirement being that a fixed level set of ϕ coincides with the front at each time t, a common choice is the signed distance from the front. Let us denote Ω^+ and Ω^- the subsets of the domain separated by the front, $I_{\Omega^\pm}(\mathbf{x})$ be the indicator of set $\Omega^\pm$ and be $d(\mathbf{x};\, \Gamma)$ the distance of point $\mathbf{x}$ from the front. The signed distance is the function defined by:

$$d_s(\mathbf{x}) = I_{\Omega^+}(\mathbf{x})\, d(\mathbf{x};\, \Gamma) - I_{\Omega^-}(\mathbf{x})\, d(\mathbf{x};\, \Gamma)\,. \tag{4}$$

Written as in eq. (4), $d_s(\mathbf{x})$ is positive in Ω^+ and negative in Ω^-. Unfortunately, the property of the level set function being a distance function is not preserved during advection. To enhance the accuracy, it is common to resort to reinitialization procedures. Numerical experiments presented hereafter will show how the techniques introduced in this work have less strict needs in terms of regularity of the level set function: we would like to point out that all tests were run *without* any kind of reinitialization.

3 Discontinuous Galerkin Approximation

3.1 DG-FE Formulation of Level Set Problem

Discontinuous Galerkin methods were originally developed for the numerical solution of hyperbolic conservation laws. Basically, the intent was to provide an approximation exhibiting a better behaviour in the presence of discontinuous solutions. Experience has proven, however, that also in the presence of a regular solution one can profit from it in terms of a reduction of the amount of numerical viscosity necessary for the purpose of stabilization. The essential feature of DG-FE methods is to decouple the degrees of freedom belonging to every element and to achieve element coupling weakly through the introduction of inter-element boundary terms. In the sequel we give a short and intuitive introduction for the case under study, referring the interested reader

to the literature (a complete review can be found in [3]). First consider the linear hyperbolic problem obtained from (2) when (3) holds:

$$\phi_t + \mathbf{b}(\mathbf{x}, t) \cdot \nabla\phi = 0. \tag{5}$$

For the moment we assume that the advection field $\mathbf{b}$ is continuous. Let $\mathcal{T}_h$ be a 1-irregular triangulation of the domain Ω. A 1-irregular mesh is a mesh with at most one irregular ("hanging") node per side. With the aim of writing the discontinuous Galerkin approximation of the original problem, we proceed formally multiplying eq. (5) by a test function $v_h \in V_h$ and integrating over an element $K \in \mathcal{T}_h$:

$$\int_K v_h \frac{\partial \phi_h}{\partial t} d\mathbf{x} + \int_K v_h \mathbf{b}(\mathbf{x}, t) \cdot \nabla\phi_h \, \mathrm{d}\mathbf{x} = 0 \quad \forall v_h \in V_h.$$

We take V_h as the space of functions whose restriction to every element K of the triangulation is a polynomial of degree at most k, possibly discontinuous on ∂K. In symbols:

$$V_h = \left\{ v_h \in L^2(\Omega) \mid v_h|_K \in \mathbb{P}_k(K) \quad \forall K \in \mathcal{T}_h \right\}.$$

Summing over $K \in \mathcal{T}_h$ we get:

$$\sum_{K \in \mathcal{T}_h} \int_K v_h \frac{\partial \phi_h}{\partial t} \, \mathrm{d}\mathbf{x} + \sum_{K \in \mathcal{T}_h} \int_K v_h \mathbf{b}(\mathbf{x}, t) \cdot \nabla\phi_h \, \mathrm{d}\mathbf{x} = 0 \quad \forall v_h \in V_h.$$

Application of Green's formula to the second integral on the right hand side gives:

$$\int_K v_h \mathbf{b} \cdot \nabla\phi_h \, \mathrm{d}\mathbf{x} = \int_{\partial K} v_h \phi_h \mathbf{b} \cdot \mathbf{n} \, \mathrm{d}\sigma - \int_K \phi_h \mathbf{b} \cdot \nabla v_h \, \mathrm{d}\mathbf{x} - \int_K v_h \phi_h \nabla \cdot \mathbf{b} \, \mathrm{d}\mathbf{x},$$

where the dependence of $\mathbf{b}$ was dropped for the sake of brevity. In all test cases we'll assume that:

$$\nabla \cdot \mathbf{b} = 0$$

will invariably hold. At this point we can introduce the jump and average operators defined as in [8]. Be e an internal edge shared by elements K^+ and K^- and let

$$f^\pm := f(\mathbf{x})|_{K^\pm}, \quad \varphi^\pm := \varphi(\mathbf{x})|_{K^\pm}$$

be the restrictions of a generic scalar or vector function to one of the two elements. Naming $\mathbf{n}^\pm(\mathbf{x})$, $\mathbf{x} \in e$ the normal to an internal edge e pointing out of $K^\pm$ we define:

$$\begin{aligned} [\![f]\!] &:= f^+\mathbf{n}^+ + f^-\mathbf{n}^-, \qquad \{f\} := \tfrac{1}{2}(f^+ + f^-), \\ [\![\varphi]\!] &:= \varphi^+ \cdot \mathbf{n}^+ + \varphi^- \cdot \mathbf{n}^-, \; \{\varphi\} := \tfrac{1}{2}(\varphi^+ + \varphi^-). \end{aligned}$$

These definitions can be extended to boundary edges, where all functions are single-valued:

$$[\![f]\!] := f^* \mathbf{n}, \quad \{f\} := f,$$

where f^* accounts for weak imposition of Dirichlet boundary conditions, as will be discussed later in this section. The sum of boundary integrals over the elements of the triangulation can be re-written as a sum over the edges. To this purpose, naming $\mathcal{E}^0$ the set of internal edges, $\mathcal{E}^\partial$ the set of boundary edges we have that:

$$\begin{aligned}\sum_{K\in\mathcal{T}_h} \int_{\partial K} v_h \phi_h \mathbf{b}\cdot\mathbf{n} d\sigma = &\sum_{e\in\mathcal{E}^0} \int_e \left(v_h^+ \phi_h^+ \mathbf{b}\cdot\mathbf{n}^+ + v_h^- \phi_h^- \mathbf{b}\cdot\mathbf{n}^- \right) d\sigma \\ &+ \sum_{e\in\mathcal{E}^\partial} \int_e v_h \phi_h^* \mathbf{b}\cdot\mathbf{n} d\sigma,\end{aligned}$$

where:

$$\phi_h^* = \begin{cases} \phi_{\text{in}} \text{ if } \mathbf{b}\cdot\mathbf{n} \le 0 \\ \phi_h \text{ if } \mathbf{b}\cdot\mathbf{n} > 0 \end{cases}.$$

being ϕ_{in} the Dirichlet data on the inflow portion of the boundary.

In order to establish weak inter-element links, we notice that $\mathbf{F}^\pm := \phi_h^\pm \mathbf{b}$ are the non conservative fluxes of the unknown ϕ_h through internal side e. The problem of establishing an interaction between elements can be then solved by substituting the non-conservative fluxes with the conservative (i.e. single valued on e) upwind numerical flux defined by:

$$\mathbf{H}(\phi_h) := \mathbf{b}\{\phi_h\} + \frac{1}{2}|\mathbf{b}\cdot\mathbf{n}|[\![\phi_h]\!],$$

where $\mathbf{n}$ is either $\mathbf{n}^+$ or $\mathbf{n}^-$. In fact, it is not difficult to prove that this substitution corresponds to weakly impose the value of ϕ on the inflow portion of the element boundary. After this substitution we end up with:

$$\begin{aligned}\sum_{K\in\mathcal{T}_h} \int_K v_h \frac{\partial \phi_h}{\partial t}\, \mathrm{d}\mathbf{x} - &\sum_{K\in\mathcal{T}_h} \int_K \phi_h \mathbf{b}\cdot\nabla v_h \, \mathrm{d}\mathbf{x} \\ &+ \sum_{e\in\mathcal{E}^0} \int_e \mathbf{b}\cdot[\![v_h]\!]\{\phi_h\} + \frac{1}{2}|\mathbf{b}\cdot\mathbf{n}|[\![v_h]\!]\cdot[\![\phi_h]\!] \, \mathrm{d}\sigma \qquad (6) \\ &+ \sum_{e\in\mathcal{E}^\partial} \int_e \mathbf{b}\cdot[\![v_h]\!]\{\phi_h^*\} \, \mathrm{d}\sigma = 0.\end{aligned}$$

The final discrete problem was obtained from the semi-discrete problem by resorting to a Runge-Kutta method of order $k+1$ for time discretization. For the details we once again refer the reader to [3].

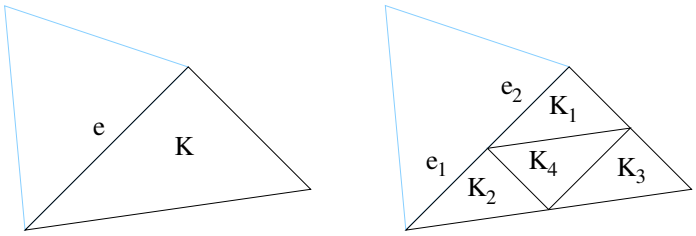

Figure 1. An example of 1-irregular mesh.

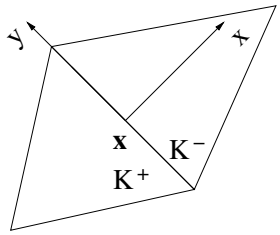

Figure 2. Frame for the computation of numerical fluxes on boundary quadrature point $\mathbf{x}$.

3.2 Non-conforming Triangulations and Isotropic Adaptivity

In this section we wish to point out some interesting features of DG-FE approximation. Assuming that the shape functions can be discontinuous on element boundary has the important consequence that non-conforming triangulations and p-adaptivity can be handled with ease. In particular:

- The degree of approximation inside each element is independent, which allows for p-adaptivity.
- Hanging nodes are allowed. As a matter of fact, consider the example in Fig. 1, where $e = e_1 \cup e_2$. Exploiting the additivity of the integral we can write the integral over e as a sum of the integrals over e_1 and e_2. After splitting the integral over edge e, it will never appear in the sum over element edges in eq. (6): this simple strategy allows easy handling of 1-irregular meshes.

The last remark is of some importance, because it makes non-conforming isotropic mesh refinement possible (see again Fig. 1). The advantage of isotropic mesh refinement is that the quality of the initial mesh is preserved irrespectively from the number of refinements and that the mesh generation is failure free. In §5 we will outline an adaptive method based on hierarchical elements on unstructured meshes.

To close this section, we give a trace for the case when the velocity field is discontinuous. The problem is now that both the velocity field and the unknown are discontinuous: in order to compute the flux on a generic interface node $\mathbf{x} \in e$, $e \in \mathcal{E}$ we move to the frame centered in $\mathbf{x}$ with x-axis parallel to $\mathbf{n}^+(\mathbf{x})$ as depicted in Fig. 2. The upwind flux is then chosen by solving

the one-dimensional Riemann problem obtained by projecting in the $\mathbf{n}^+$ direction the original problem. This method automatically allows weak handling of boundary conditions, since they can simply be treated as one of the states of the Riemann problem.

4 Subgrid edge stabilization for cFEM approximation

It is well known that the standard Galerkin method fails when the solution of advection dominated equations or pure advection equation is considered [9]. As discussed in the previous section, one remedy consists in resorting to discontinuous Galerkin methods, for which stability and local mass conservation is built into the method. On the other hand, if a continuous finite element approximation is used, a suitable stabilization of the Galerkin formulation is required. The discontinuous Galerkin method takes the form of an interior penalty method whereas for the continuous case a Petrov-Galerkin approach is used. This dichotomy was questioned in a recent paper [10] and it was shown that it is possible to construct interior penalty methods which are stable for the transport equation and of optimal order for both conforming and non-conforming finite element spaces. In the case of continuous approximations a term must be added to the standard Galerkin formulation penalizing the jump of the gradient over internal element boundaries. In the present work, we consider a local version of this interior penalty stabilization approach, that will be referred to as *subgrid edge stabilization*. This method was introduced and analysed in [1].

We consider a family of quasi-uniform triangulation $(\mathcal{T}_H)_H$, of the domain Ω, where the parameter $H = \max_{K_H \in \mathcal{T}_H} H_K$ characterizes the mesh refinement. From each triangle $K_H \in \mathcal{T}_H$, four triangles are created by connecting the midpoints of the edges. We set $h = H/2$ and denote by $K_h \in \mathcal{T}_h$ the resulting finer triangulation. A two-level piecewise linear finite element approximation is defined by introducing the following two spaces:

$$
\begin{aligned}
X_H &= \{\phi_H \in (W^0_{\boldsymbol{b}}(\Omega) \cap H^1(\Omega)) \mid \phi_{H|K_H} \in \mathbb{P}_1(K_H), \forall K_H \in \mathcal{T}_H\},\\
X_h &= \{\phi_h \in (W^0_{\boldsymbol{b}}(\Omega) \cap H^1(\Omega)) \mid \phi_{h|K_h} \in \mathbb{P}_1(K_h), \forall K_h \in \mathcal{T}_h\},
\end{aligned}
$$

where the functional space $W^0_{\boldsymbol{b}}$ is given by

$$
W^0_{\boldsymbol{b}}(\Omega) = \{\psi \in L^2(\Omega) \mid (\boldsymbol{b}(\boldsymbol{x},t)\cdot\nabla\psi) \in L^2(\Omega) \mid \psi|_{\partial\Omega^-} = 0\},
$$

with $\partial\Omega^- = \{\boldsymbol{x} \in \partial\Omega \mid \boldsymbol{b}(\boldsymbol{x},t)\cdot\boldsymbol{n}(\boldsymbol{x}) < 0\}$.

The subgrid edge stabilization consists in adding a term which penalizes the jump of the gradient *only* over the edges of the subtriangles K_h internal to

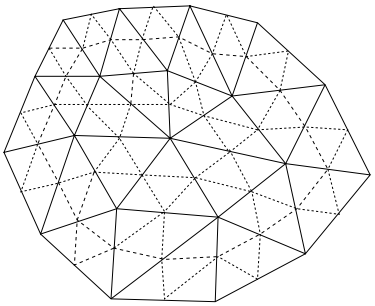

Figure 3. Subgrid internal edges (dashed line) where the stabilization term is added.

K_H (see Fig. 3), defined on each K_H as

$$\mathcal{E}_i(K_H) = \{e_i \in \partial K_h \mid e_i \notin \partial K_H, \forall K_h \in K_H\}\,.$$

The continuous finite element discretization of problem (5) then reads: find $\phi_h \in X_h$ such that

$$\int_\Omega v_h \frac{\partial \phi_h}{\partial t} d\mathbf{x} + \int_\Omega v_h \mathbf{b}\,(\mathbf{x},t) \cdot \nabla \phi_h \; \mathrm{d}\mathbf{x} + j(v_h, \phi_h) = 0, \quad \forall v_h \in X_h,$$

where we have introduced the stabilization term $j(v_h, \phi_h)$ defined by

$$j(v_h, \phi_h) = \sum_{K_H} \sum_{e_i \in \mathcal{E}_i} \int_{e_i} h_{e_i}^2 [\nabla v_h][\nabla \phi_h]\, d\sigma,$$

with $[f] := f^+ - f^-$ denoting the standard jump operator.

It has been shown in [1] that the subgrid edge stabilization can be cast in the framework of the subgrid viscosity stabilization proposed in [11]. In particular, stability and optimal error estimates have been proven based on a norm equivalence argument.

The same approach can be extended to higher order finite elements. For quadratic approximations, it is possible (see [1]) to derive a subgrid edge stabilization with optimal error estimates by adding the following term

$$j(v_h, \phi_h) = \sum_{K_H} \sum_{e_i \in \mathcal{E}_i} \int_{e_i} \left(h_{e_i}^2 [\nabla v_h][\nabla \phi_h] + h_{e_i}^3 [\boldsymbol{D}^2 v_h][\boldsymbol{D}^2 \phi_h] \right) d\sigma,$$

where $\boldsymbol{D}^2(\cdot)$ denotes the Hessian operator. Note that in this case an additional term controlling the jump of the second derivatives is required.

One of the major advantages of interior penalty methods, as opposed to Petrov-Galerkin type stabilizations such as SUPG, relies in the complete freedom in the choice of time discretization. Since the stabilization term is independent of time, we may use lumped mass and high order time-stepping schemes. In the present work, the fully discretized problem is obtained by

considering a second order Backward Difference Formula (BDF2) scheme for the time discretization.

The subgrid edge stabilization has been found to guarantee good mass conservation properties, as shown in the numerical results reported in §6. Indeed, given the local nature of the proposed technique, the stabilization is only present on the finest scales and hence on the macro scale the method will have the same conservation properties as the standard Galerkin method.

5 Mesh Adaptivity and Refinement Criteria for DG-FEM Approximation

As mentioned before, the DG-FE approximation makes mesh adaptivity easy to handle. In order to adapt the mesh, however, a local error estimate is necessary: we then look for a local error estimate which is computable from known quantities and which can drive the choice of elements to refine or derefine.

Several techniques to derive *a posteriori* error estimates have been presented in the literature. In [13] an *a posteriori* error estimate for linear and non linear hyperbolic problems is developed using a duality argument. In that work the authors suggest that the estimate obtained by solving the dual problem is remarkably more accurate than the one obtained by further bounding it so to eliminate the dual solution. When applied to unsteady problems, however, this requires solving the dual problem at each time step. Moreover, the approximation space for the dual problem must be denser than that for the primal. Other error estimates, like those developed in [14] or [15], are applicable only to certain classes of problems or are compatible only with special and less generalizable solution methods.

In consideration of the previous remarks, and recalling the aim of the present work, we preferred to rely on a more heuristic approach, which proved effective in all the numerical experiments. As will be shown in §6, the behaviour of DG-FEM approximation rapidly enhances when increasing the order of polynomial space k. This observation suggested us to employ a more accurate solution $v_h^q \in V_h^q$ to estimate the local error of a less accurate solution $v_h^p \in V_h^p$, $p < q$. Suppose that the exact solution u has Sobolev regularity s, i.e. $u \in H^s(\Omega)$, $s \geq 2$, and two approximate solutions u_h^p and u_h^q are available corresponding respectively to approximations of order p and q, with $s-1 \geq q = p+\sigma,\ \sigma \geq 1$. Then:

$$\|u - u_h^p\|_{L^2(K)} \leq \|u_h^q - u_h^p\|_{L^2(K)} + \|u - u_h^q\|_{L^2(K)}\,, \tag{7}$$

where we use $\|.\|_{L^2(K)}$ for the spatial L^2 norm. Since at every time step the coarser solution is obtained by evolving the projection of the finer solution to the space V_h^p, we can concentrate on a single step. We now exploit the fact

that (see, e.g., [16]):

$$\left\|u - u_h^k\right\|_{L^2(K)} \leq Ch^{k+1/2} \left\|u\right\|_{H_x^{q+1}(\Omega)} ,$$

which tells us that, having assumed $p < q$, the first term in the right hand side of (7) scales with $h^{p+1/2}$, while the second scales with $h^{q+1/2}$. We therefore assume that:

$$\|u - u_h^q\|_{L^2(K)} \ll \|u_h^q - u_h^p\|_{L^2(K)} ,$$

and that:

$$\|u - u_h^p\|_{L^2(K)} \sim \|u_h^q - u_h^p\|_{L^2(K)} .$$

We would finally like to point out that in most of the works dealing with level set techniques mesh adaptation is done only in the neighbourhood of the front: in our case this strategy would not prove effective since we decided to avoid using any form of reinitialization, and, had we only refined around the front, error could be brought in from other regions of the domain.

In order to reduce the computational cost of the higher order solution, hierarchical bases were used, so that the local matrices corresponding to the lower polynomial degree can be extracted from those corresponding to the higher polynomial degree. Moreover, at every time step the restriction of the more accurate solution to the less dense space was used to advance the less accurate solution. Grid adaptation was handled by resorting to a nested mesh structure.

6 Numerical Results

6.1 Non Adaptive Methods

In this subsection we compare the results obtained with the methods presented above in the non-adaptive version. In order to assess the mass conservation properties, we consider the rotating square and the Zalesak notched disk test cases. Besides conserving the mass, an interface tracking method should be accurate in the presence of thin tails. In this respect, to evaluate the performance of the proposed methods, we considered the deformation and stretching of a circular bubble under the effect of a shear flow. In the sequel we give a short description of all the test cases.

Rotating square. The first test case we consider the rigid body rotation of the signed distance function from a 0.2×0.2 square due to a constant vorticity field centered in $(0.8, 0.2)$:

$$u = \frac{\pi}{2}(y - 0.2) , \quad v = -\frac{\pi}{2}(x - 0.8) .$$

The main difficulty in this test is that the advected interface has sharp corners, which are smeared out by dissipative methods. We used it both as an indicator of the mass conservation properties of the methods proposed and as a benchmark against classic stabilization methods.

Zalesak disk. The Zalesak test case consists in predicting the rigid body rotation of the signed distance function from a notched disk. The initial interface is a circle centered at $(0.5, 0.75)$ with a radius of 0.15 and notch dimensions of 0.05×0.25 ($[W \times H]$). The velocity field is vortex centered in the midpoint of the unit square $[0, 1]^2$, defined by:

$$u = 2\pi\,(y - 0.5)\,, \quad v = -2\pi\,(x - 0.5)\,,$$

where normalization was applied so that one revolution per unit time is performed. This test case is somehow more severe than the previous one, since it has two difficulties: the presence of sharp corners, which are smoothed out, and the notch, which tends to disappear when the numerical dissipation is too high.

Shear flow. In the last test case we consider the deformation of a circular bubble of radius 0.15 centered in $(0.5, 0.75)$ due to the velocity field given by:

$$u = \sin(2\pi y)\sin(\pi x)^2, \quad v = -\sin(2\pi x)\sin(\pi y)^2.$$

The main difficulty of this test consists in the progressive formation of a thin tail, which requires high accuracy to be followed correctly. In order to have an estimate of the accuracy of the method, the velocity field is reverted for $t \geq 1$ and the solution is deformed back. The comparison with initial conditions serves as a qualitative measure of the results.

The tests were run on different meshes and, for the DG-FE approximation, different polynomial degrees were used. In order to make the comparison fair we used two discretizations with roughly 5000 and 13000 degrees of freedom respectively and compared solutions with a similar computational cost. To better appreciate the results, comparison was provided with a cFEM implementation stabilized with SUPG method.

All numerical tests show that the methods proposed in this paper behave well in terms of both mass conservation and accuracy, even in the presence of sharp corners or large deformations. Data related to the mass conservation properties are given in Tab. 6.1, while all solutions are plotted in Fig. 4–9. As regards DG-FE approximation in particular, for a given number of unknowns, increasing the polynomial degree enhances the performance in all considered test cases. The results obtained with the IP stabilized cFEM approximation clearly show the advantages of the proposed method when compared to classical stabilization approaches such as SUPG, both in term of accuracy and mass

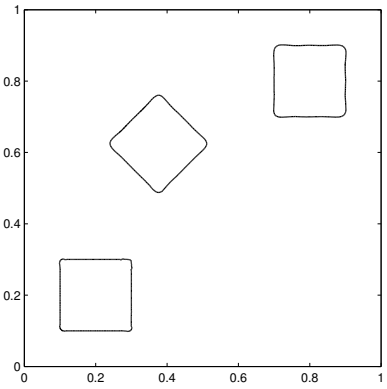

(a) $(\mathbb{P}_1, 1800, 5400)$.

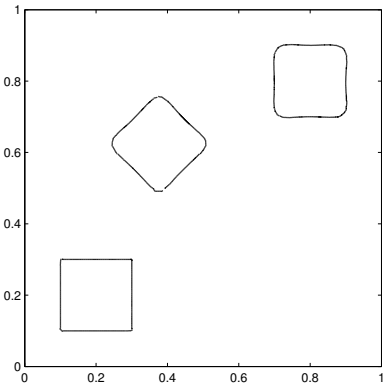

(b) $(\mathbb{P}_1, 4418, 13254)$.

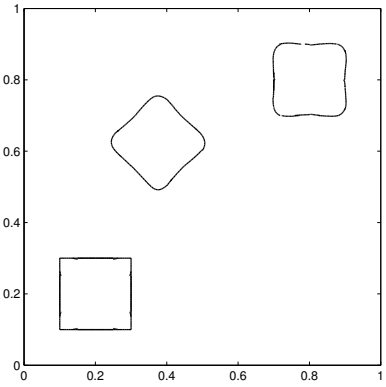

(c) $(\mathbb{P}_2, 800, 4800)$.

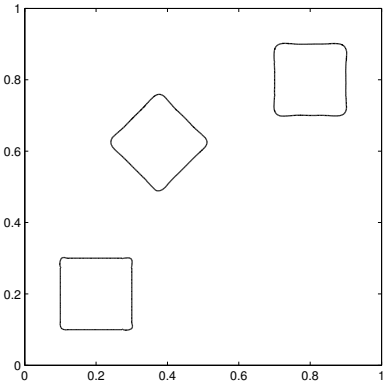

(d) $(\mathbb{P}_2, 2178, 13068)$.

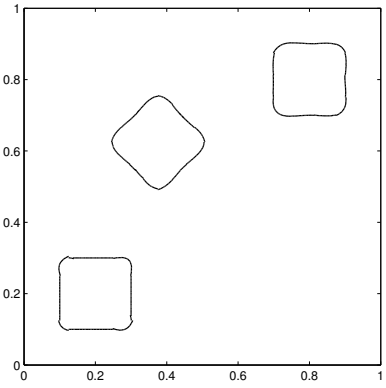

(e) $(\mathbb{P}_3, 512, 5120)$.

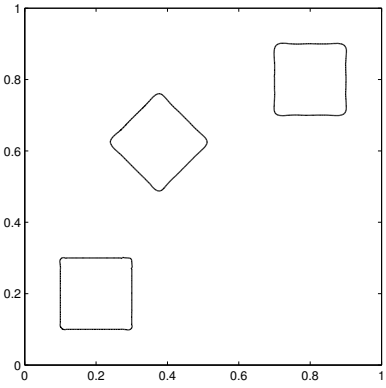

(f) $(\mathbb{P}_3, 1352, 13520)$.

Figure 4. DG-FE solution of rotating square problem (*FE space*, *Number of elements*, *Number of DOFs*). Solution plots at times 0, 0.5, 1.

Case	t	SUPG		IP-cFEM		$\mathbb{P}_1$ DG-FE		$\mathbb{P}_2$ DG-FE		$\mathbb{P}_3$ DG-FE	
		Coarse	Fine	Coarse	Fine	Coarse	Fine	Coarse	Fine	Coarse	Fine
Rot. Sq.	0	100	100	100	100	100	100	100	100	100	100
	0.5	89.74	93.84	100.10	100.00	101.32	98.58	101.79	101.08	100.61	96.82
	1	78.90	87.78	100.08	100.01	101.14	98.99	99.48	100.53	99.13	100.2
Zalesak	0	100	100	100	100	100	100	100	100	100	100
	0.2	109.25	107.09	98.32	98.78	104.80	99.17	103.53	101.21	98.55	99.89
	0.4	108.01	99.84	97.04	99.16	100.3	107.56	101.33	104.52	97.77	99.81
	0.6	88.15	102.64	100.22	98.45	111.49	101.09	104.58	101.30	97.54	99.27
	0.8	76.76	96.08	100.91	99.34	114.50	102.02	106.24	100.74	97.76	98.79
	1	66.23	89.24	101.44	100.16	118.45	102.91	104.89	100.42	99.49	99.76
Shear	0	100	100	100	100	100	100	100	100	100	100
	0.2	109.25	107.09	98.32	98.78	104.80	99.17	103.53	101.21	98.55	99.89
	0.4	108.01	99.84	97.04	99.16	100.3	107.56	101.33	104.52	97.77	99.81
	0.6	88.15	102.64	100.22	98.45	111.49	101.09	104.58	101.30	97.54	99.27
	0.8	76.76	96.08	100.91	99.34	114.50	102.02	106.24	100.74	97.76	98.79
	1	66.23	89.24	101.44	100.16	118.45	102.91	104.89	100.42	99.49	99.76

Table 1
Percentage of mass preserved at chosen times (non-adaptive methods).

	t	N_E	$\mathbb{P}_2$-DOFs	mean (ϵ_K)	var (ϵ_K)	% mass
Rot. Sq.	0.5	1196	7176	0.76	0.41	104.49
	1.0	1187	7122	0.74	0.41	99.53
Zalesak	0.2	1274	7644	0.78	0.34	99.38
	0.4	1214	7284	0.80	0.32	99.47
	0.6	1196	7176	0.80	0.33	99.41
	0.8	1238	7428	0.78	0.34	98.90
	1.0	1214	7284	0.80	0.32	98.45
Shear	0.5	1031	6186	–	–	99.57
	1.0	1067	6402	–	–	100.55
	1.5	1187	7122	–	–	99.58
	2.0	1175	7050	–	–	98.82

Table 2
Number of elements, $\mathbb{P}_2$-DOFs, mean and standard deviation of the effectivity indices (where analytical solution is available) and percentage of mass preserved (adaptive DG-FE method).

conservation. It should be noted that better results can be obtained if a fully consistent SUPG implementation is used in the framework of space-time finite element approximations. For a detailed discussion on this subject, and for an analysis of the dependence on the stabilization parameter for both subgrid edge and SUPG stabilizations, we refer to [1].

6.2 h-adaptive DG-FEM

In this section we report the results of the numerical test for the adaptive DG-FE method. We set $p_K = 1$ and $q_K = 2$ for all the elements. A maximum number of 1300 elements is fixed. To test the efficiency of our estimator we introduce the effectivity index ϵ_K as the ration between the L^2-norm $\hat{e}_u$ of our estimator and the L^2-norm e_u of the true error: $\epsilon_K = \frac{\hat{e}_u}{e_u}$. In Tab. 2 are reported some results about the numerical tests described above: number of

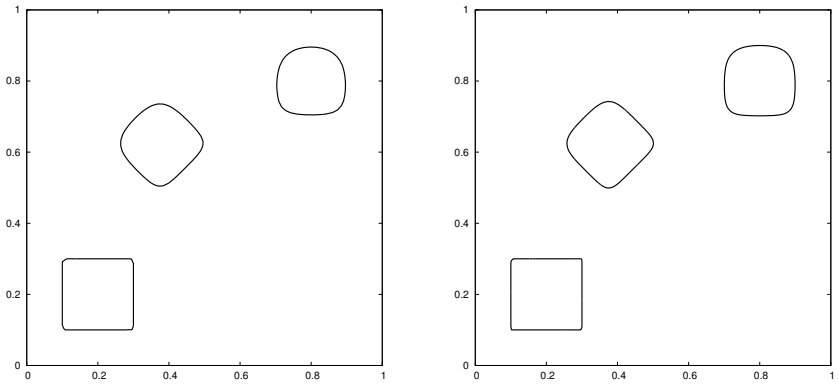

(a) (SUPG, 4800) (b) (SUPG, 13300)

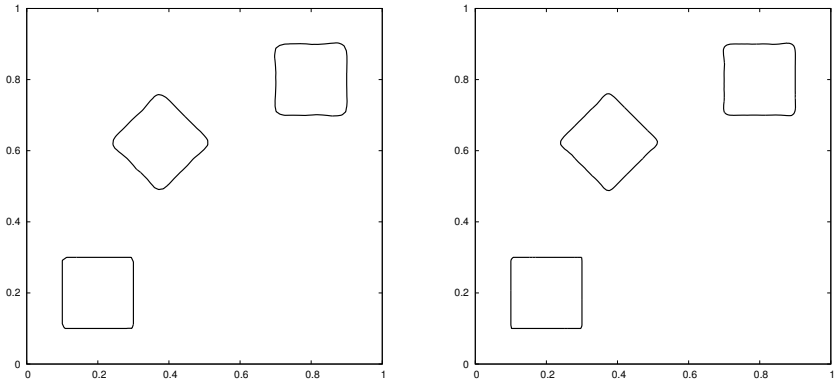

(c) (IP, 4800) (d) (IP, 13300)

Figure 5. cFEM solution of rotating square problem with SUPG and IP stabilization (*Stabilization method*, *Number of DOFs*).Solution plots at times 0, 0.5, 1.

elements, number of $\mathbb{P}_2$ degrees of freedom (DOFs), mean and standard deviation over the grid elements of the effectivity index (where an analytical solution is available) and percentage of mass preserved at chosen time steps. Plots of the solutions are given in Fig. 10.

7 Conclusions

In this paper we presented two mass-preserving finite element implementations of the level set method, one based on a DG-FE approximation, the other on a continuous FE approximation with an interior penalty subgrid edge stabilization. Both methods achieve stability by weakly imposing suitable features on the solution, and cure the illnesses of classical FE approximations. The methods were tested on a set of widely known problems, showing their good behaviour both in terms of mass conservation and accuracy. For the DG-FE approximation an h-adaptive version was presented, whose aim was to enhance

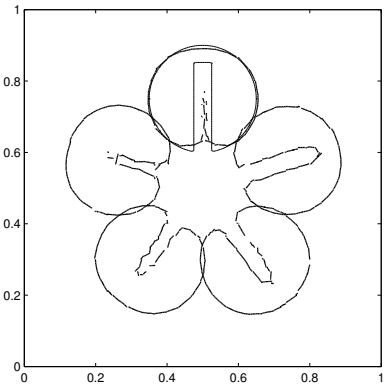

(a) $(\mathbb{P}_1, 1800, 5400)$.

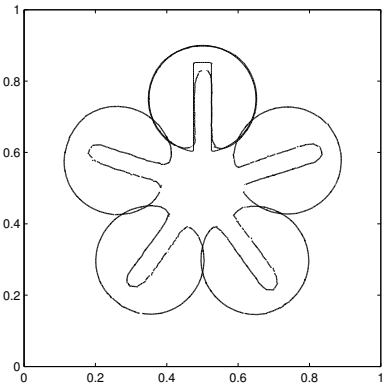

(b) $(\mathbb{P}_1, 4418, 13254)$.

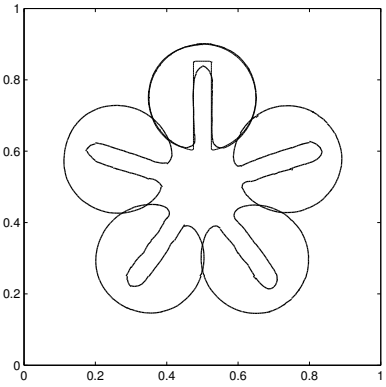

(c) $(\mathbb{P}_2, 800, 4800)$.

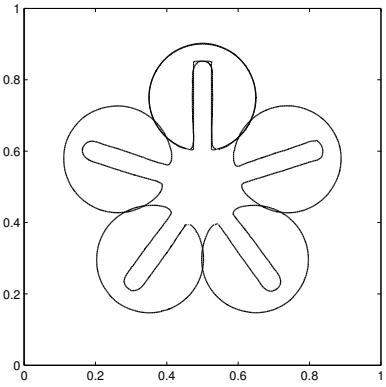

(d) $(\mathbb{P}_2, 2178, 13068)$.

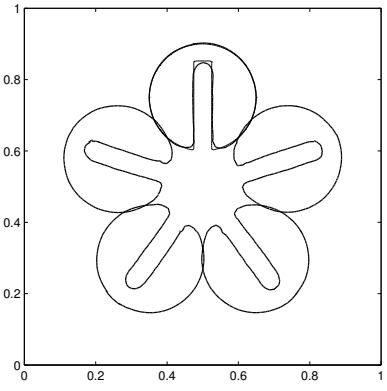

(e) $(\mathbb{P}_3, 512, 5120)$.

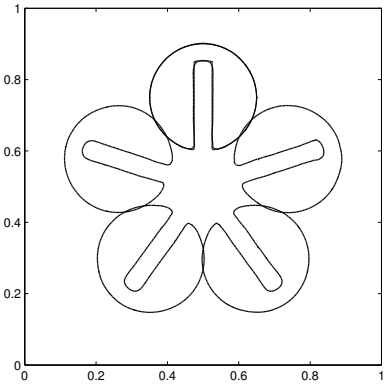

(f) $(\mathbb{P}_3, 1352, 13520)$.

Figure 6. DG-FE solution of Zalesak rotating disk problem (*FE space*, *Number of elements*, *Number of DOFs*). Solution plots at times 0.2, 0.4, 0.6, 0.8, 1.

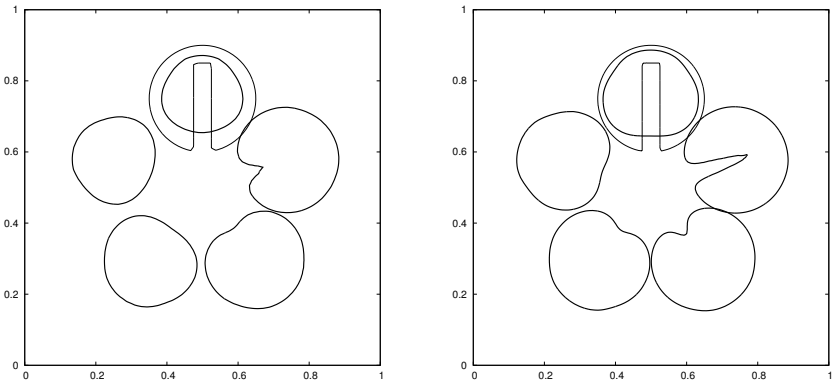

(a) (SUPG, 4800) (b) (SUPG, 13300)

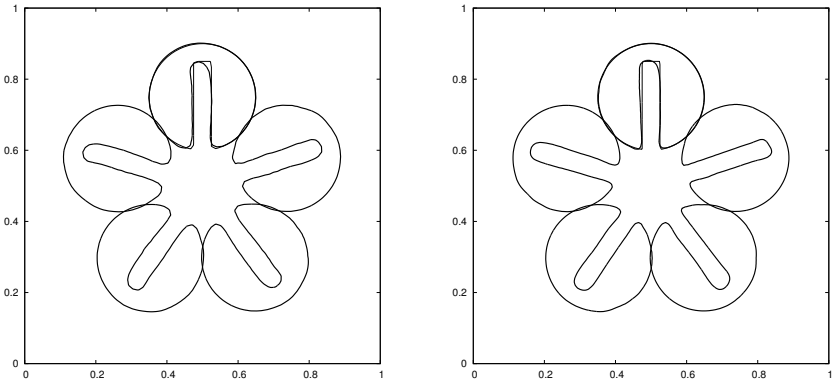

(c) (IP, 4800) (d) (IP, 13300)

Figure 7. cFEM solution of Zalesak rotating disk problem with SUPG and IP stabilization (*Stabilization method*, *Number of DOFs*). Solution plots at times 0.2, 0.4, 0.6, 0.8, 1.

the results and to lower the computational cost. Comparison between the IP and the various flavours of the DG-FE method was made fair by running the test cases on discretizations with roughly the same number of unknowns. In all cases the methods behaved well, giving similar results and thus proving that mass conservation and accuracy can be achieved without the need to resort to spurious strategies.

Acknowledgements

The authors would like to thank Prof. F. Bassi, Dr. E. Burman and Prof. F. Saleri for the fruitful discussions which greatly improved the present work.

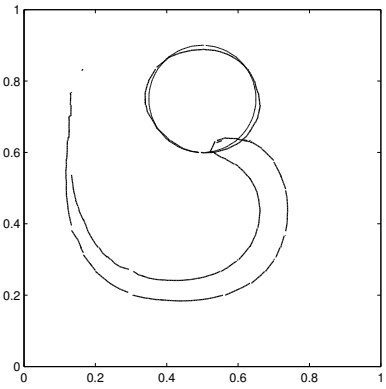

(a) $(\mathbb{P}_1, 1800, 5400)$.

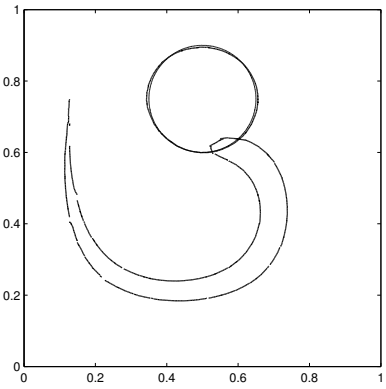

(b) $(\mathbb{P}_1, 4418, 13254)$.

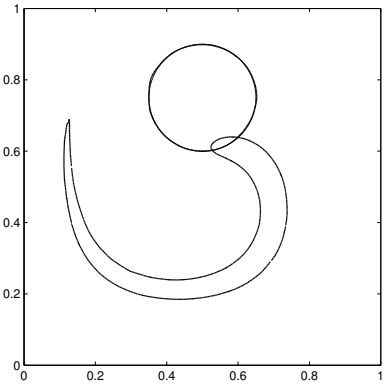

(c) $(\mathbb{P}_2, 800, 4800)$.

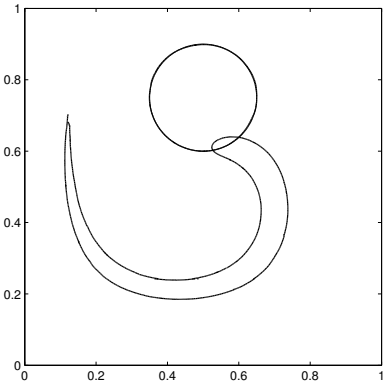

(d) $(\mathbb{P}_2, 2178, 13068)$.

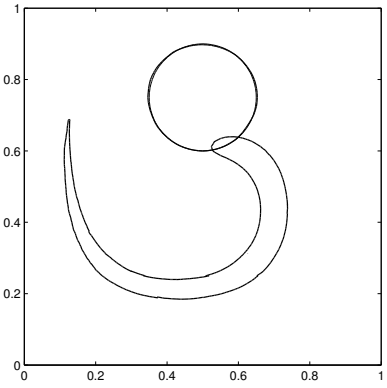

(e) $(\mathbb{P}_3, 512, 5120)$.

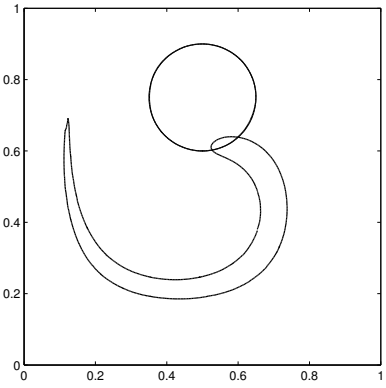

(f) $(\mathbb{P}_3, 1352, 13520)$.

Figure 8. DG-FE solution of shear flow problem (*FE space*, *Number of elements*, *Number of DOFs*). Solution plot at times 0, 1, 2.

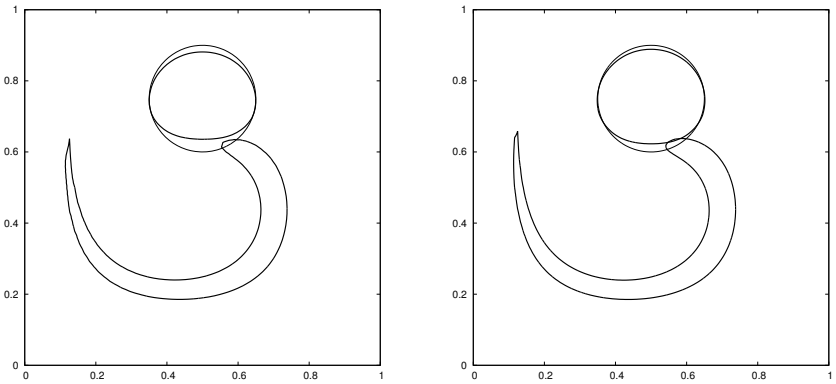

(a) (SUPG, 4800) (b) (SUPG, 13300)

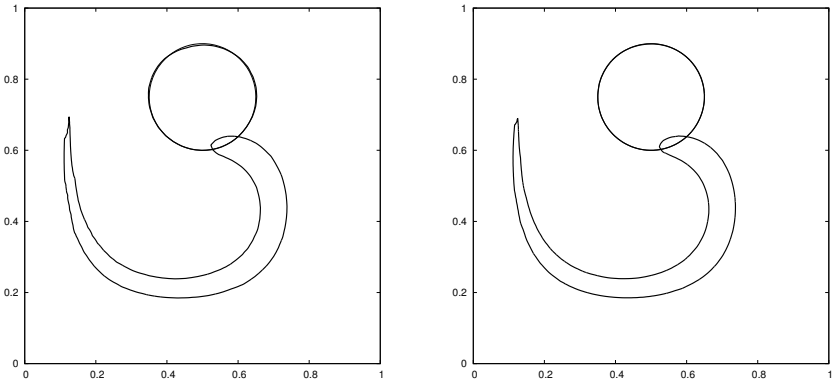

(c) (IP, 4800) (d) (IP, 13300)

Figure 9. cFEM solution of shear flow problem with SUPG and IP stabilization (*Stabilization method*, *Number of DOFs*).Solution plot at times 0, 1, 2.

References

[1] N. Parolini, Computational Fluid Dynamics for naval engineering application, Ecole Polytechnique Fédérale de Lausanne, Thesis No 3138 (2004).

[2] D. Enright, R. Fedkiw, J. Ferziger, I. Mitchell, A Hybrid Particle Level Set Method for Improved Interface Capturing, J. Comput. Phys. **183**, pp. 83-116, 2002.

[3] B. Cockburn, C. W. Shu, Runge-Kutta discontinuous Galerkin methods for convection-dominated problems, J. Sci. Comp. **16**, No. 13, pp. 173–261, 2001.

[4] A. Dervieux and F. Thomasset, Approximation methods for Navier–Stokes problems, Lecture Notes in Mathematics, vol. 771, ch. A finite element method for the simulation of Rayleigh-Taylor instability, pp. 145–158, Springer-Verlag, Berlin, 1980.

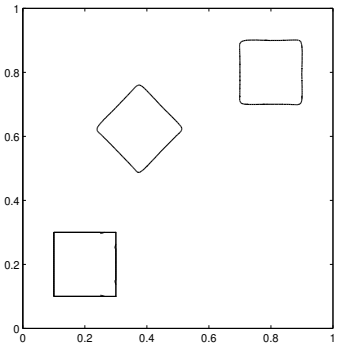

(a) (0, 0.5, 1.0)

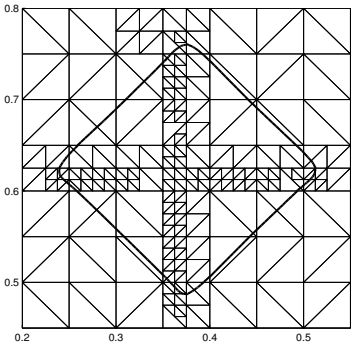

(b) (0.5)

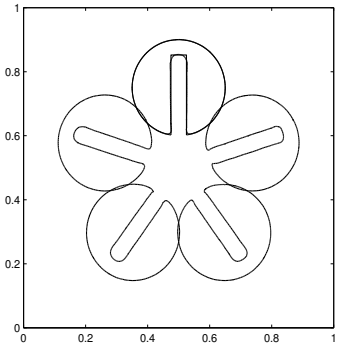

(c) (0.2, 0.4, 0.6, 0.8, 1.0)

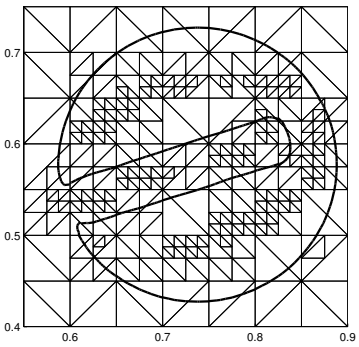

(d) (0.2)

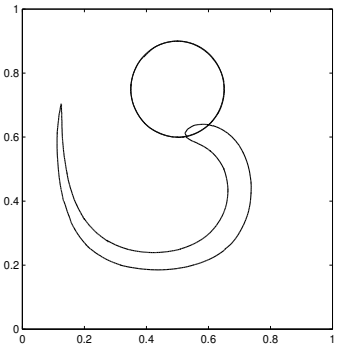

(e) (0, 1.0, 2.0)

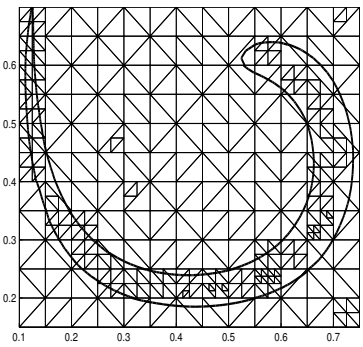

(f) (1.0)

Figure 10. hDG-FE solutions of the three test cases (*time*): solution plots (left) and detail of a computational grid (right).

[5] S. Osher, J. A. Sethian, Fronts propagating with curvature dependent speed: Algorithms based on Hamilton-Jacobi formulations, J. Comput. Phys. **79**, pp. 12–49, 1988.

[6] J. A. Sethian, Level set methods and fast marching methods, 2^{nd} edition, Cambridge Press, 1999.

[7] E. Burman, P. Hansbo, Edge stabilization for Galerkin approximations of convection-diffusion-reaction problems, Comput. Methods Appl. Mech. Engrg. **193**, pp. 1437–1453, 2004.

[8] D. N. Arnold, F. Brezzi, B. Cockburn, L. D. Marini, Unified analysis of discontinuous Galerkin methods for elliptic problems, SIAM J. Num. Anal. **39**, pp. 1749–79, 2001.

[9] C. Johnson, Numerical solution of partial differential equations by the finite element method, Cambridge University Press, 1987.

[10] E. Burman, A unified analysis for conforming and nonconforming stabilized finite element methods using interior penalty, SIAM J. Numer. Anal. (2004). To appear.

[11] J.-L. Guermond, Stabilization of Galerkin approximation of transport equations by subgrid modeling, Math. Model. Numer. Anal. **33**, pp. 1293–1316, 1999.

[12] S. Zalesak, Fully multidimensional flux-corrected transport algorithms for fluids, J. Comp. Phys. **31**, pp. 335–362, 1979.

[13] P. Houston, E. Süli, *hp*-adaptive discontinuous Galerkin finite element methods for first order hyperbolic problems, SIAM J. Sci. Comput. **23**, No. 4, pp. 1226–1252, 2001.

[14] L. Krivodonova, J. E. Flaherty, Error estimation for discontinuous Galerkin solutions of two-dimensional hyperbolic problems. Challenges in computational mathematics (Pohang, 2001), Adv. Comput. Math. **19**, No. 1-3, pp. 57–71, 2003.

[15] K. S. Bey, J. T. Oden, *hp*-version discontinuous Galerkin methods for hyperbolic conservation laws, Comput. Methods Appl. Mech. Engrg., Vol. **133**, No. 3–4, pp. 259–286, 1996.

[16] C. Johnson, J. Pitkäranta, An analysis of the discontinuous Galerkin method for a scalar hyperbolic equation, Math. Comp. **46**, No. 173, pp. 1–26, 1986.